American Journal of Engineering and Applied Sciences

Original Research Paper

Synthesis and Characterization of Au@TiO_2 NWs and their Catalytic Activity by Water Splitting: A Comparative Study with Degussa P25

[1]Abniel Machín, [1]María Cotto, [1]José Ducongé,
[1]Juan C. Arango, [2]Carmen Morant, [1]Francisco Márquez

[1]School of Natural Sciences and Technology, Universidad del Turabo, Gurabo, PR00778, USA
[2]Department of Applied Physics and Instituto Nicolás Cabrera,
Universidad Autónoma de Madrid, Madrid, Spain 28049, Spain

Article history
Received: 28-05-2017
Revised: 01-06-2017
Accepted: 05-06-2017

Corresponding Author:
Francisco Márquez
School of Natural Sciences and Technology, Universidad del Turabo, Gurabo, PR00778, USA
Email: fmarquez@suagm.edu

Abstract: Different amount of gold nanoparticles (1, 3, 5, 10 wt%) were deposited on the surface of synthesized titanium oxide nanowires (TiO_2 NWs) and Degussa P25 (TiO_2-P25). The results evidenced the presence of small and dispersed gold particles on the surface of TiO_2 NWs and TiO_2-P25 and an increase in the specific surface area of all the composites. The photocatalytic activity was characterized by measuring the hydrogen production by water splitting, using UV-vis radiation. Au@TiO_2 NWs catalysts showed the highest production of hydrogen (1,436 μmol hg^{-1}), with a gold loading of 10 wt%, while in the case of Au@TiO_2-P25 the hydrogen production was slightly lower (800 μmol hg^{-1}), with a gold loading of 5 wt%. The enhancement in the hydrogen production was 11.5 times higher than that reported by the TiO_2 NWs catalyst (125 μmol hg^{-1}) and 5.2 times higher than the TiO_2-P25 (154 μmol hg^{-1}). The activity of the catalysts was found to be dependent both on the surface area of the composites and on the amount of gold.

Keywords: Hydrogen Production, TiO_2 Nanowires, Gold Nanoparticles, Photocatalysis, Water Splitting

Introduction

One of the most important challenges of the 21st century is the development of sustainable energy systems, capable of fulfilling a constantly growing energy demand and, at the same time, be environmentally friendly. Multiple efforts have been made in order to cut or reduce the dependency of fossil fuels as the primary source of energy. In those efforts, hydrogen has been proposed as the perfect candidate to replace fossil fuels, due to the following reasons: (1) is the most abundant element in the universe and can be found in water and biomass; (2) has a higher energy yield (122 kJg^{-1}) compared to gasoline (40 kJg^{-1}); (3) Is environmentally friendly because does not produce greenhouse gases, sulfur oxides or any harmful effect on the environment; and (4) can be stored as gas, liquid or solid (Balat, 2008; Dunn, 2012; Mazloomi and Gomes, 2012). Even though hydrogen has all the mentioned benefits, the actual production is mainly derived from fossil fuels, preventing it of becoming competitive (Mazloomi and Gomes, 2012).

Since the landmark discovery of photoelectro-chemical water splitting by Fujishima and Honda (1972), researchers from all over the world have been developing systems able to produce clean hydrogen. Among all the materials that have been used, titanium oxide (TiO_2) is one of the most promising due to its nontoxicity, low cost and high chemical stability (Liao *et al*., 2012; Stroyuk *et al*., 2009; Primo *et al*., 2011; Kudo and Miseki, 2008; Ortega *et al*., 2014). One of the main disadvantage of using TiO_2 as a photocatalyst to produce hydrogen via water splitting is its wide band gap energy (i.e., 3.2 eV for anatase). With this energy gap, only UV light can be used. This fact must be taken into consideration since only 4% of the total radiation that comes from the Sun is in the UV region, whereas 50% is in the visible region of the electromagnetic spectrum (Liao *et al*., 2012). It is for that reason that recent investigations are focused on modifying the band gap of

the catalyst. Some of the chemical modifications include the doping of TiO_2 with metal and nonmetallic elements (Stroyuk *et al*., 2009; Primo *et al*., 2011; Kudo and Miseki, 2008; Ortega *et al*., 2014; Yuzawa *et al*., 2012; Tanaka *et al*., 2012; Padikkaparambil *et al*., 2013). The incorporation of noble metals, such as platinum (Pt), gold (Au) and silver (Ag), on the surface of titanium oxide, has been gaining a lot of interest in recent years due to the ability of the noble metal nanoparticles in reducing the fast recombination of the photogenerated charge carriers, enabling the use of visible light (Fang *et al*., 2012; Naseri *et al*., 2011; Lakshminarasimhan *et al*., 2007; Jose *et al*., 2013; Naldoni *et al*., 2013; Chen *et al*., 2011). By reducing the photogenerated charge carriers, the UV activity is increased due to the electron transfer from the Conduction Band (CB) of TiO_2 to the noble metal nanoparticles (Chen *et al*., 2011). The photoactivity in the visible range of the electromagnetic spectrum can be explained due to the surface plasmon resonance effect and charge separation by the transfer of photoexcited electrons from the metal nanoparticles to the CB of TiO_2 (Jose *et al*., 2013; Naldoni *et al*., 2013; Chen *et al*., 2011; Gomes-Silva *et al*., 2011; Murdoch *et al*., 2011; Baatz *et al*., 2008; Oros-Ruiz *et al*., 2013).

Among noble metals, gold has gained much attention since the 80's because of its wide range of applications, including electronics, photodynamic therapy, delivery of therapeutic agents, sensors, probes, diagnostics and catalysis (Primo *et al*., 2011; Ortega *et al*., 2014; Yuzawa *et al*., 2012; Tanaka *et al*., 2012; Padikkaparambil *et al*., 2013; Fang *et al*., 2012; Naseri *et al*., 2011; Gomes-Silva *et al*., 2011). Different approaches have been developed in order to incorporate gold Nanoparticles (Au NPs) on the surface of TiO_2. For example, Nijishima *et al*. (2010) reported the adsorption of preformed Au colloids; Lu *et al*. (2012) and Wang *et al*. (2012) used a photodeposition method, Shen *et al*. (2012) used an impregnation process and Kuo *et al*. (2013) a chemical reduction approach.

The reduction and incorporation of a gold salt on TiO_2, using a reducing agent such as sodium borohydride ($NaBH_4$), has been widely used due to its simplicity and fast results. Lin *et al*. (2013) studied the size effect of Au NPs on the catalytic reduction of p-nitrophenol with $NaBH_4$ and found that the particle size of the Au nanoparticles depended on the $NaBH_4$ added to the reaction mixture. On the other hand, Naldoni *et al*. (2013) reported a high H_2 evolution using $NaBH_4$ as reducing agent. Furthermore, they reported that the reduction of a gold salt with $NaBH_4$ produces highly dispersed metal nanoparticles in intimate contact with TiO_2. Moreover, the product exhibits better photocatalytic properties than pure titania, confirming that this technique is suitable for preparing highly active photocatalysts.

In the present research, titanium oxide nanowires (TiO_2 NWs) in the rutile crystalline phase were synthesized. This material, along with the commercial titanium oxide Degussa P25 (TiO_2-P25), were used as support for incorporating Au NPs on the surface, using a chemical reduction method with $NaBH_4$ as reducing agent. These gold-based catalysts were tested for the water splitting reaction, with hydrogen production, under UV-vis irradiation. Different experimental parameters, such as gold loading, surface area and irradiation time, were taking into account to study the efficiency of the catalytic process. The titania gold-based catalysts were characterized by using SEM/EDS, HRTEM, UV-vis spectroscopy, BET surface area, XRD, Raman and GC-TCD.

Materials and Methods

Reagents

All reagents were used as received. Acetone, isopropyl alcohol +99.9% and HCl 37% (ACS Reagent), were provided by Acros Chemicals. $TiCl_4$ 99.9% was obtained from Fisher Scientific. Degussa P25 (Degussa, nanopowder with 21 nm particle size, 35-65 m^2g^{-1} surface area, +99.5%), $HAuCl_4.3H_2O$ (ACS Reagent, +49.0% Au basis) and $NaBH_4$ +99.9%, were provided by Sigma Aldrich. All the experimental solutions were prepared using ultra-pure water (Milli-Q water, 18.2 $M\Omega cm^{-1}$ at 25°C). Si <100> substrates p-type boron doped, provided by El-CAT, were used as substrates for the hydrothermal growth of TiO_2 NWs. For photocatalytic experiments, Na_2S 99.9% and Na_2SO_3 +98%, obtained from Sigma Aldrich, were used as sacrificial reagents.

Synthesis of TiO_2 NWs

The synthesis of the TiO_2 NWs was made following the method described by Cotto *et al*. (2013). In a typical synthesis, 50 mL of concentrated hydrochloric acid and 50 mL of deionized water were mixed in a 200 mL Erlenmeyer flask. After that, 3 mL of the titanium precursor was added by dripping, under agitation at room temperature. The mixture was magnetically stirred until all solid particles were dissolved (approximately 10 min). Then, the solution was placed into 30 mL Teflon-lined stainless steel autoclaves. Next, single crystal silicon substrates, Si<100>, were introduced inside the autoclaves. Autoclaves were maintained at 180°C for 2 h. The resulting TiO_2 NWs, grown on the surface of the silicon wafers, were toughly washed with deionized water and dried overnight at 60°C.

Synthesis of the Au@TiO_2 Catalysts

The deposition of Au NPs on the surface of TiO_2 NWs and TiO_2-P25 is based on the method described by

Naldoni *et al*. (2013). A typical synthesis consisted on the dispersion of 500 mg of the desired catalyst in 40 mL of H_2O and further sonication for 20 min. After that, the desired amount of the gold precursor was added to the reaction mixture and stirred for 30 min. Finally, a $NaBH_4$ solution (10 mg in 10 mL of H_2O) was added dropwise, under stirring and allowed to react for 10 min at room temperature. The reaction product was centrifuged, washed three times with deionized water and dried overnight at 60°C. The different Au@TiO_2 NWs composites were identified as 1%Au@TiO_2 NWs, 3%Au@TiO_2 NWs, 5%Au@TiO_2 NWs and 10%Au@TiO_2 NWs. In the case of Au@TiO_2-P25, the catalysts were identified as 1%Au@TiO_2-P25, 3%Au@TiO_2-P25, 5%Au@TiO_2 -P25 and 10%Au@TiO_2 -P25. The numbers correspond to the weight percentage of gold nanoparticles in the sample.

Characterization of the Catalysts

The catalysts were fully characterized by Scanning Electron Microscopy (SEM), using a JEOL JSM6010LV, operating at 20 kV, coupled to an Energy Dispersive Spectrometer (EDS), Field Emission Scanning Electron Microscopy (FE-SEM), using a Philips XL30 S-FEG and High Resolution Transmission Electron Microscopy (HR-TEM), using a Jeol 3000F. Brunauer Emmett Teller (BET) specific surface areas were measured using a Micromeritics ASAP 2020, according to N_2 adsorption isotherms at 77 K. Raman measurements were acquired with a DXR Thermo Raman microscope, employing a 532 nm laser source at 5 mW power and a nominal resolution of 5 cm^{-1}. X-Ray Diffraction (XRD) patterns were obtained in theta/2theta configuration in the range of 20-80° at 2° min^{-1}, using a Bruker D8 Advance X-ray diffractometer, operating at 40 kV and 40 mA. The UV-vis was measured using a Shimadzu UV-2401PC.

Photocatalytic Experiments

The photocatalytic hydrogen production was measured as follows: 100 mL of deionized water was added to a 200 mL quartz reactor flask. Then 50 mg of the gold-based catalyst was added to the flask containing the water. Solutions of 0.5 M Na_2S and 0.03 M Na_2SO_3 were added as sacrificial reagents. The reaction mixture was thermostatized at 20°C, magnetically stirred at 20 rpm and purged with nitrogen for at least 20 min. Then, the solution was exposed to UV-vis radiation for 120 min using different filters to select the appropriate irradiation wavelength. The produced hydrogen was collected, using nitrogen as gas carrier, identified and quantified by Gas Chromatography with a Thermal Conductivity Detector (GC-TCD, Perkin-Elmer Clarus 600).

Results and Discussion

Characterization of TiO_2-P25 Catalyst

The titanium oxide P25 (TiO_2-P25) is a commercial catalyst. The manufacturer (Sigma Aldrich) reports that the content of the catalyst is a mixture of 70% anatase and 30% rutile. Chen *et al*. (2011) argue that TiO_2-P25 typically shows greater activity than pure anatase or pure rutile for most photocatalytic reactions. They explain that the transference of photo-excited electrons from the conduction band of rutile to that of anatase across interfacial heterojunctions and hole migration from the valence band of anatase to that of rutile, facilitates charge separation and increases the number of charge carriers available for photoreactions. The specific surface area, as determined by the BET method, was found to be 55 m^2g^{-1}. Figure 1 shows the SEM image of TiO_2-P25. As can be seen there, the catalyst consists of aggregates of irregular spherical shaped-particles of ca. 50-75 nm in size.

Characterization of TiO_2 NWs Catalyst

As shown in Fig. 2A and 2B, the as-synthesized nanowires consisted of homogeneous and highly branched structures. The high surface area of this material (373 m^2g^{-1}) may be justified as due partly to the contribution of the highly-branched structures and could have relevant effects on the catalytic properties of this material. At higher magnification (Fig. 2C and 2D), it can be seen that it consists of a randomly arranged material with different domains and sizes.

TEM (Fig. 3) was used to further study the morphology and crystallinity of the TiO_2 NWs. As can be seen there, TiO_2 NWs is characterized by having high aspect ratio, with lengths of several hundred nanometers (Fig. 3A). Figure 3D presents rutile crystalline structure, showing a lattice spacing of ca. 0.32 nm between adjacent lattice planes. Based on the studies published by Chen *et al*. (2011), the spacing measured in Fig. 3D corresponds to the (101) plane of the rutile lattice.

Characterization of the Au@TiO_2 Catalysts

Different amounts (1, 3, 5, 10 wt%) of Au NPs were deposited on the surface of the catalysts by chemical reduction using $NaBH_4$. Figure 4 shows the FE-SEM image of the 10%Au@TiO_2-P25 at a magnification of 100,000x. After gold incorporation, the morphology of the catalysts did not change much, but smaller particles were observed possibly due to the disaggregation of the pristine support. For this reason, Au NPs are not easily distinguished in Fig. 4. 10%Au@TiO_2-P25 consists of very small particles (<100 nm) with irregularly distributed gold nanoparticles throughout the sample. It can be inferred that the diameter of the gold nanoparticles is less than 20 nm.

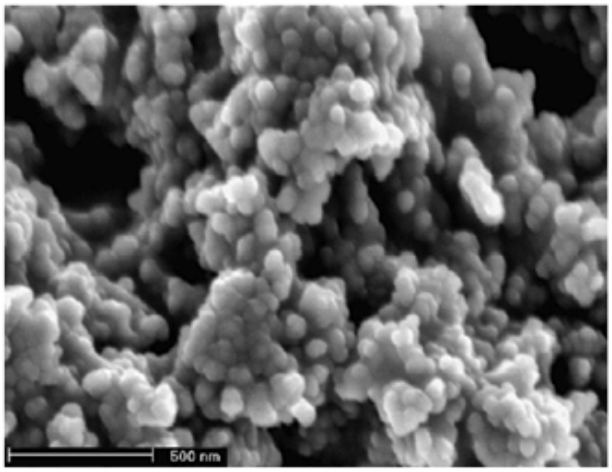

Fig. 1. SEM image of TiO_2-P25 at 60,000x

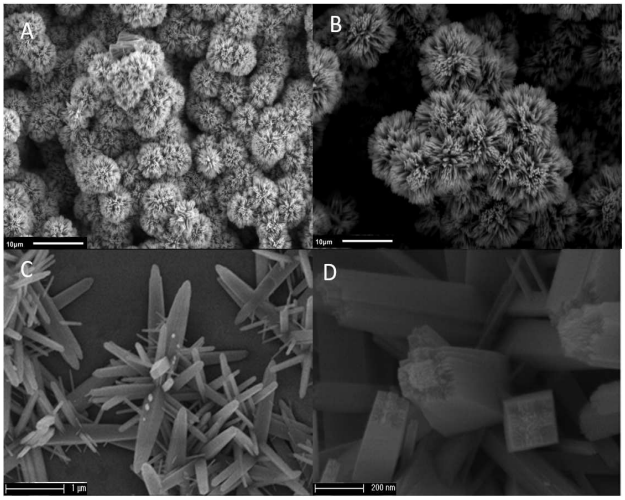

Fig. 2. SEM images of the as-synthesized TiO_2 NWs at different magnifications: 2,500x (A); 5,000x (B); 33,000x (C); and 50,000x (D)

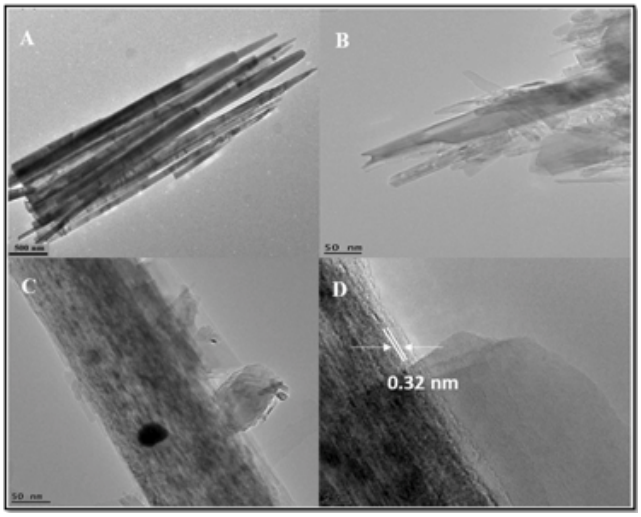

Fig. 3. TEM images of the as-synthesized TiO_2 NWs at different magnifications

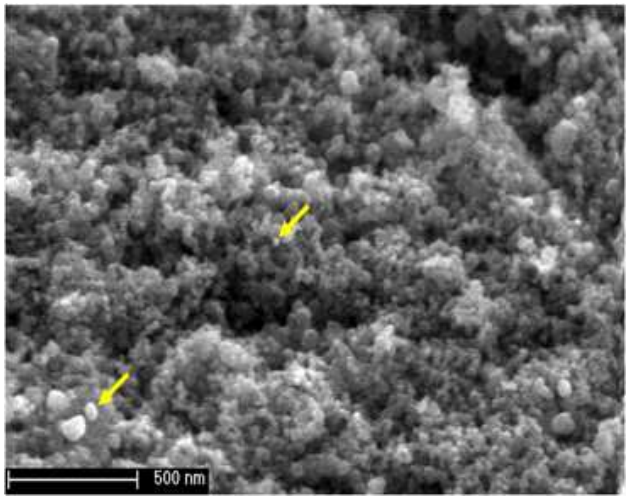

Fig. 4. FE-SEM image of the 10%Au@TiO_2-P25 at a magnification of 100,000x

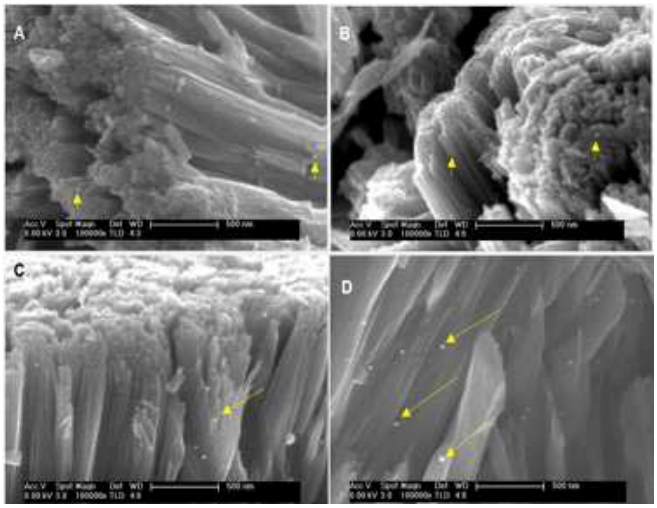

Fig. 5. FE-SEM images of 1%Au@TiO_2 NWs (A), 3%Au@TiO_2 NWs (B), 5%Au@TiO_2 NWs (C) and 10%Au@TiO_2 NWs (D) catalysts at different magnifications. The arrows indicate the Au NPs

In the case of the TiO_2 NWs, the presence of Au NPs on the surface of 1%Au@TiO_2 NWs (Fig. 5A) and 3%Au@TiO_2 NWs (Fig. 5B) was practically not detected. In the case of the catalysts 5%Au@TiO_2 NWs (Fig. 5C) and 10%Au@TiO_2 NWs (Fig. 5D), small, spherical and homogeneous gold particles, with sizes below 20 nm, were observed on the surface of the nanowires. Gold nanoparticles with less than 5 nm diameter usually exhibit high photocatalytic activity under visible light irradiation, mainly due to the excitation of Surface Plasmon Resonance (SRP) (Murdoch *et al*., 2011). Previous studies demonstrated that $NaBH_4$ is one of the most appropriate reducing agents, promoting the formation of small gold nanoparticles (Naldoni *et al*., 2013).

Figure 6 shows a TEM image of the 10%Au@TiO_2 NWs catalyst. As can be seen there, the samples consisted of wires of irregular shapes of ca. 300-500 nm length. Thus, the reduction treatment apparently did not induce any significant modification of the nanomaterial morphology. The gold nanoparticles were grown homogenously, showing spherical shapes with diameters less than 50 nm. These results are in agreement with those obtained by FE-SEM. As mentioned above, gold nanoparticles with less than 20 nm are predicted to exhibit higher catalytic activity (Haruta *et al*., 1987).

The BET surface area of Au@TiO_2 catalysts with different Au loadings were analyzed (Table 1). It can be seen that for the TiO_2-P25 the incorporation of Au NPs increased the surface area, compared to unmodified TiO_2-P25 (55 m^2g^{-1}). However, a decrease of 14 m^2g^{-1} between the 5%Au@TiO_2-P25 (83 m^2g^{-1}) and 10%Au@ TiO_2-P25 (69 m^2g^{-1}) catalysts was observed. This behavior suggests that possibly the most suitable gold loading for this adduct may range from 5 wt% to less than 10 wt%.

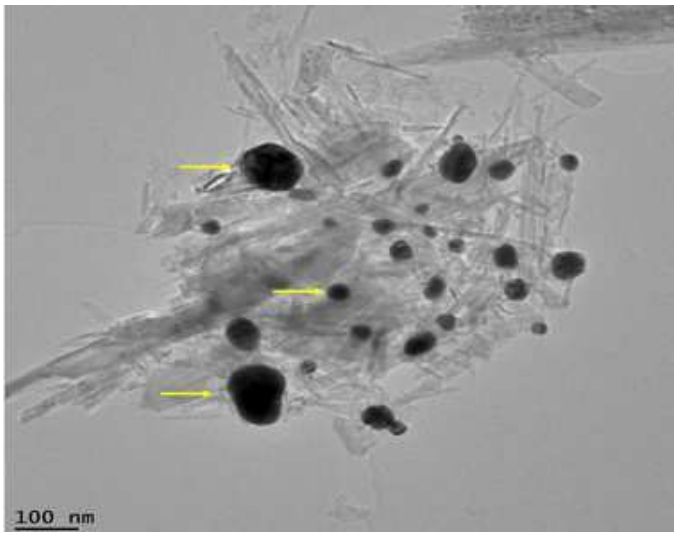

Fig. 6. TEM image of 10%Au@TiO_2 NWs catalyst. The arrows indicate the Au NPs

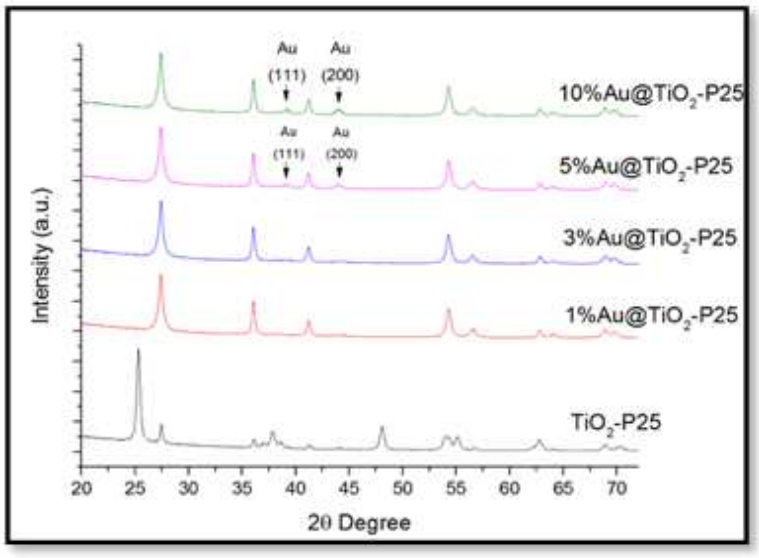

Fig. 7. XRD diffraction patterns of the TiO_2-P25, 1%Au@TiO_2-P25, 3%Au@TiO_2-P25, 5%Au@TiO_2-P25 and 10%Au@TiO_2-P25 catalysts

Table 1. BET surface area of the Au@TiO_2 catalysts.

	TiO_2-P25 (m^2g^{-1})	TiO_2 NWs (m^2g^{-1})
Without Au	52	373
1%Au	58	374
3%Au	74	384
5%Au	83	402
10%Au	69	431

Before gold deposition (Table 1), the average surface area of the as-synthesized TiO_2 NWs was 373 m^2g^{-1}. As in the case of the commercial catalyst (TiO_2-P25), the incorporation of gold nanoparticles onto the pristine catalyst resulted in the increase of the specific surface area. This effect is much more significant in composites with higher percentage of gold on the surface, showing increases of about 29 m^2g^{-1} (5%Au@TiO_2 NWs) and 58 m^2g^{-1} (10%Au@TiO_2 NWs), respectively. As determined by FE-SEM, these nanoparticles are highly dispersed on the surface of the catalysts, suggesting that the chemical reduction approach is an efficient method to synthesize these composites.

The XRD patterns of the Au@TiO_2 catalysts are shown in Fig. 7. TiO_2-P25 is a mixture of 70% anatase and 30% rutile. The characteristic peaks of anatase (JCPDS 21-1272) can be found at ca. 25° (101), 38°

(004), 48° (220), 54° (105) and 55° (211) (Hanoar and Sorrell, 2011), while the rutile crystalline phase has its characteristic peaks at ca. 27° (110), 36° (101), 41° (111) and 54° (211) (JCPDS 34-180) (Manveen and Verma, 2014; Hanoar and Sorrell, 2011). All the peaks corresponding to both anatase and rutile are present in the diffraction pattern of Fig. 7. On the other hand, the intensities of all peaks were those that would be expected from a mixture of 70% anatase and 30% rutile. For the Au@TiO_2-P25 composites, the incorporation of Au NPs caused a shift towards higher angles in all the gold composites when compared with the unmodified TiO_2-P25 catalyst. The characteristic peak of rutile (ca. 27°) was not present in any gold loadings. Kowalska *et al*. (2012) reported similar results and explain that this decrease in the intensity could be attributed to the presence of gold nanoparticles with higher sizes and different shapes. Two peaks corresponding to gold at ca. 38° (111) and 44° (200), were identified at gold loadings of 5 and 10 wt%, respectively. As expected, the intensity of the peaks increased at higher gold loadings.

Figure 8 shows the diffraction patterns of pristine and modified TiO_2 NWs. As can be seen there, these catalysts show the most intense peaks at 27° (110), 36° (101) and 55° (211), that have been unambiguously ascribed to the rutile phase (JCPDS 88-1175). The diffractograms of the Au@TiO_2 NWs showed a small shift towards lower angles when compared to the pure TiO_2 NWs. This displacement has been attributed to the incorporation of the gold nanoparticles on the surface of the support (Fang *et al*., 2012). No gold peak was observed at low gold loading (1%Au@TiO_2 NWs and 3%Au@TiO_2 NWs). In 5%Au@TiO_2 NWs, a small peak at ca. 38° has been ascribed to the presence of gold nanoparticles. This peak experienced an increase in intensity as the gold load increased, as seen in the catalyst 10% Au @ TiO_2 NWs.

Figure 9 shows the Raman spectra of the Au@TiO_2-P25 catalysts. Singh *et al*. (2014) reported that anatase phase shows major bands at ~150, 395, 515 and 638 cm^{-1}. These bands can be appreciated in all the TiO_2-P25 catalysts and have been attributed to the five Raman-active modes of the anatase phase, corresponding to $E_{g(1)}$, $B_{1g(1)}$, A_{1g} + $B_{1g(2)}$ and $E_{g(2)}$ vibrational modes. The typical Raman bands resulting from the rutile phase appear at ~143 (superimposed with the 145 cm^{-1} band from the anatase), 235, 455 and 612 cm^{-1} and can be ascribed to the B_{1g}, E_g and A_{1g} vibrational modes (Singh *et al*., 2014; Wang *et al*., 2012). Only the peak at ca. 455 cm^{-1} was observed. In the case of the Au@TiO_2-P25 catalysts the peak corresponding to the presence of gold nanoparticles was not detected in any of the Au@TiO_2-P25 catalysts. The only change observed by increasing the gold loading of the samples was a slightly decrease in the intensity of the characteristic peaks. This effect has been attributed directly to the presence of gold (Tamm *et al*., 2016).

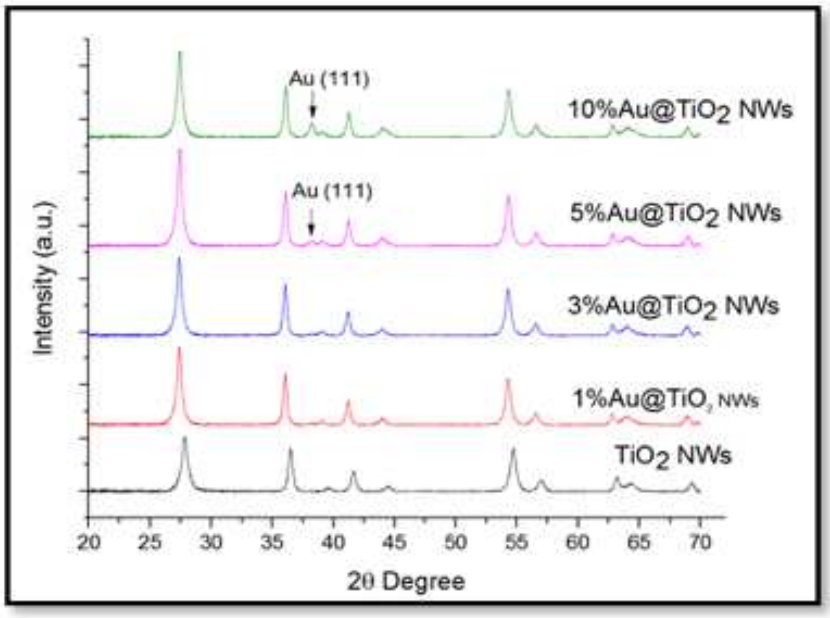

Fig. 8. XRD diffraction patterns of the TiO_2 NWs, 1%Au@TiO_2 NWs, 3%Au@TiO_2 NWs, 5%Au@TiO_2 NWs and 10%Au@TiO_2 NWs catalysts

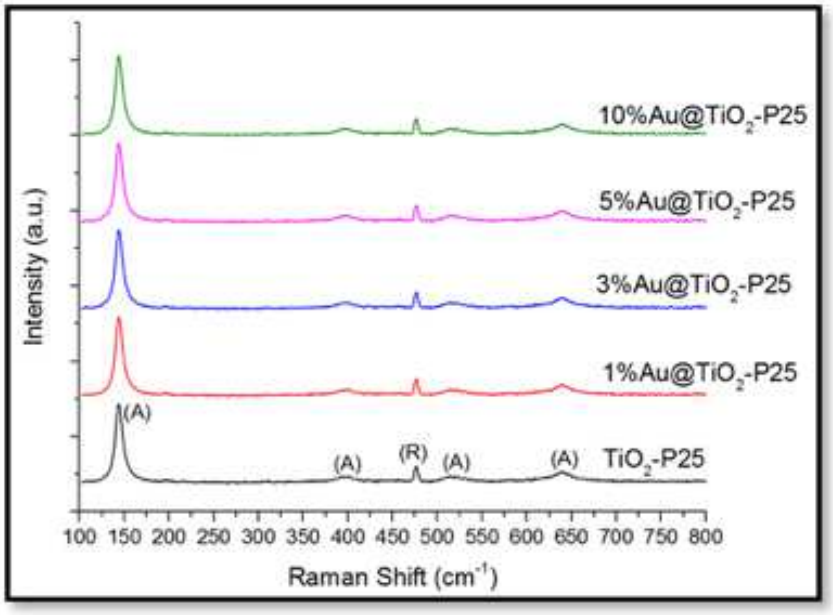

Fig. 9. Raman spectra of the TiO_2-P25, 1%Au@TiO_2-P25, 3%Au@TiO_2-P25, 5%Au@TiO_2-P25 and 10%Au@TiO_2-P25 catalysts. In TiO_2-P25, A and R indicate anatase and rutile, respectively

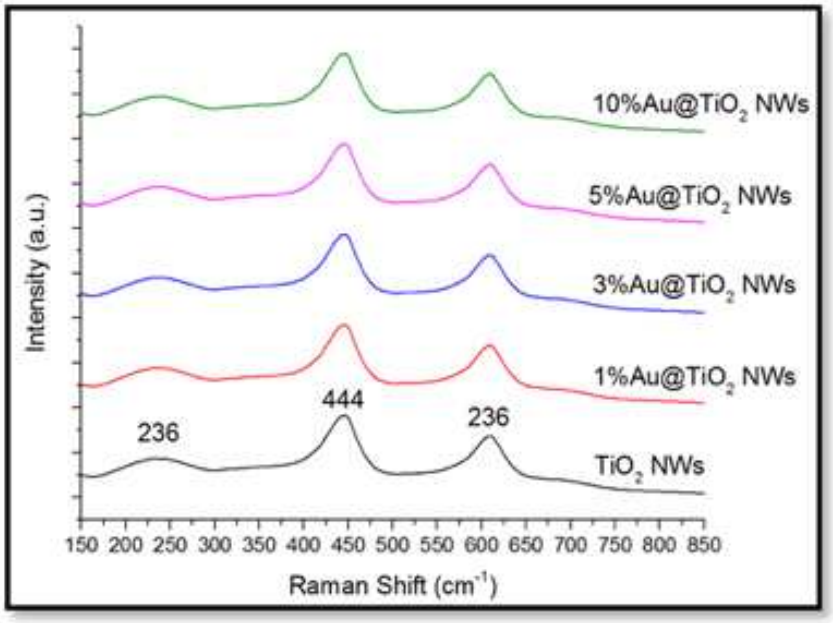

Fig. 10. Raman spectra of the TiO_2 NWs, 1%Au@TiO_2 NWs, 3%Au@TiO_2 NWs, 5%Au@TiO_2 NWs and 10%Au@TiO_2 NWs catalysts

The Raman spectra of the different Au@TiO_2 NWs catalysts are shown in Fig. 10. The characteristic Raman bands of TiO_2 rutile can be found at ca. 236, 444 and 608 cm^{-1} and two small shoulders at ca. 707 and 319 cm^{-1} (Hanoar and Sorrell, 2011). As can be seen there, all these bands are present, confirming that rutile is the only crystalline phase identified in the as-synthesized TiO_2 NWs. No bands associated with Au NPs were detected in Au@TiO_2 NWs catalysts. However, compared to the Raman spectra of the Au@ TiO_2-P25 catalysts, no peak reduction was detected for Au@TiO_2 NWs. This behavior could be due to a better distribution of the gold nanoparticles through the samples and to the high surface area of the catalysts (Luo *et al*., 2016).

The Au@TiO_2-P25 catalysts were also characterized by UV-vis spectroscopy and the results are shown in Fig.

11. The main absorption of TiO_2 is observed in the UV region of the spectrum, showing a maximum at ca. 300 nm and low absorption efficiency in the visible range. No additional absorption peaks were detected for any of the Au@TiO_2-P25 catalysts. This result might be possible due to different reasons including low sensitivity of the instrument and small size of the Au NPs (Tanaka *et al*., 2012; Fang *et al*., 2012).

Figure 12 shows the UV-vis spectra of the Au@TiO_2-NWs catalysts. No gold signal was observed in the 1%Au@TiO_2 NWs, 3%Au@TiO_2 NWs and 5%Au@TiO_2 NWs, but a small shoulder at ca. 550 nm was observed for the 10%Au@TiO_2 NWs. This shoulder was unambiguously attributed to the surface plasmon resonance (SPR) exhibited by the Au NPs (Tanaka *et al*., 2012; Fang *et al*., 2012; Chen *et al*., 2011; Gomes-Silva *et al*., 2011). The plasmon absorption depends on the size of the gold nanoparticles and arises from the collective oscillations of the free conduction band electrons that are induced by the incident electromagnetic radiation on Au NPs (Fang *et al*., 2012; Chen *et al*., 2011; Gomes-Silva *et al*., 2011).

Photocatalytic Hydrogen Production

The results of hydrogen production via water splitting obtained by Au@TiO_2-P25 catalysts under different wavelengths are shown in Figure 13. It can be clearly seen that the incorporation of different amounts of Au NPs considerably increased the amount of hydrogen produced in both the ultraviolet and visible region of the electromagnetic spectrum. The highest amount of hydrogen was 800 μmol hg^{-1} (5%Au@TiO_2-P25 at 400 nm), representing a difference of 646 μmol hg^{-1} when compared to the maximum hydrogen production of the unmodified TiO_2-P25 catalyst (154 μmol hg^{-1}). This result was expected since, of all the Au@TiO_2-P25 catalysts, 5%AuTiO_2-P25 composite obtained the highest surface area (83 m^2/g). Different studies (Hanoar and Sorrell, 2011; Luttrell *et al*., 2014; Li *et al*., 2015) have found that a key factor in the photocatalytic activity of titania is its high surface area. A high surface area leads to a higher density of localized states (Hanoar and Sorrell, 2011), which involve electrons with energies between the conduction and valence bands. Hanoar and Sorrell (2011) mention that these electrons are present due to terminated and unsaturated bonds on the surfaces, providing beneficial charge separation in the form of trapping sites for photo-generated charge carriers.

The fact that the highest amount of hydrogen was obtained at 400 nm and not at 220 nm, as it was seen for TiO_2-P25 catalyst, is an indication that the Au NPs are allowing the use of visible light to produce hydrogen. One property of the Au NPs that has been extensively studied is its Surface Plasmon Resonance (SPR) effect. The SPR is associated with a considerable enhancement of the electric near field, where the electrons from the valence band of the TiO_2 are excited to the conduction band by UV light irradiation. The electrons then migrate to the Au NP, on the surface of the TiO_2. The SPR effect induced by visible light (~500-580 nm) can boost the energy intensity of trapped electrons resulting in the photocatalytic activity enhancement (Tanaka *et al*., 2012; Fang *et al*., 2012; Chen *et al*., 2011; Haro *et al*., 2014).

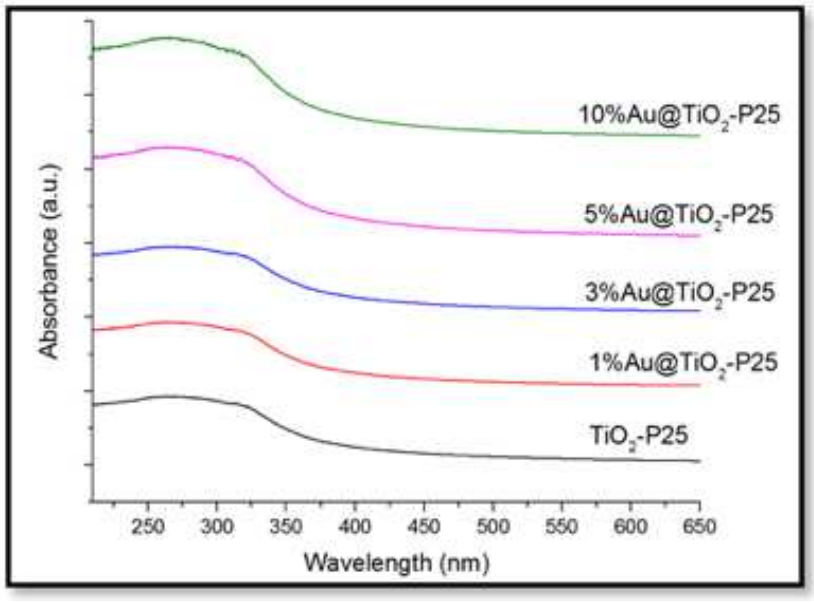

Fig. 11. UV-vis spectra of the TiO_2-P25, 1%Au@TiO_2-P25, 3%Au@TiO_2-P25, 5%Au@TiO_2-P25 and 10%Au@TiO_2-P25 catalysts

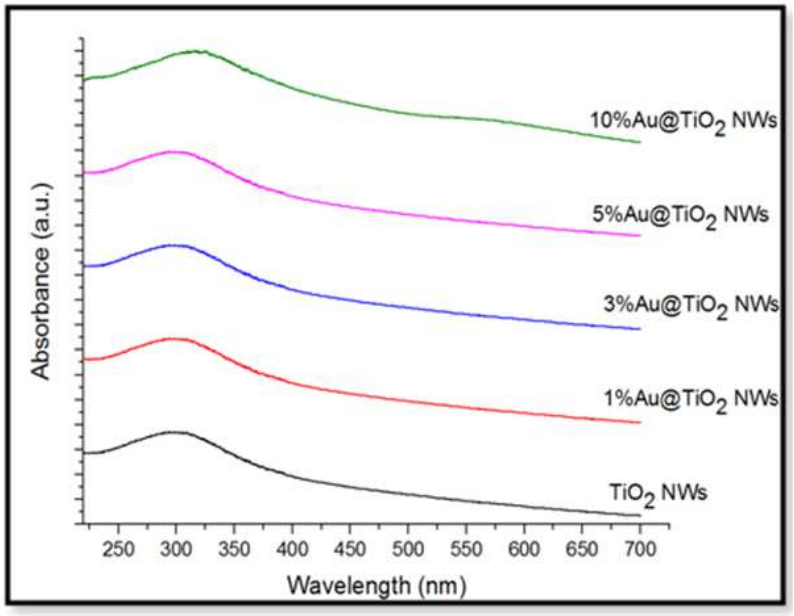

Fig. 12. UV-vis spectra of the TiO_2 NWs, 1%Au@TiO_2 NWs, 3%Au@TiO_2 NWs, 5%Au@TiO_2 NWs and 10%Au@TiO_2 NWs catalysts

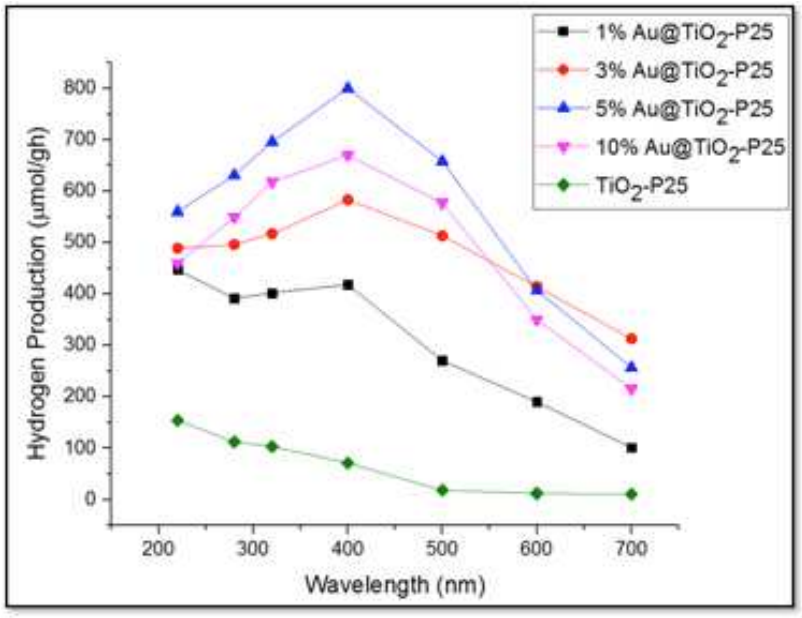

Fig. 13. Hydrogen production for the different Au@TiO_2-P25 catalysts

Recent studies (Tanaka *et al*., 2012; Chen *et al*., 2011; Oros-Ruiz *et al*., 2013) found that when Au NPs are irradiated by wavelengths ranging from 500 to 590 nm, electrons from the Au NPs are injected into the conduction band of the titanium dioxide. Those injected electrons have enough energy to reduce the water molecule and produce hydrogen, while the water molecule is oxidized on the surface of the Au NPs. This ability of the Au@TiO_2 composites to be able to use both visible and ultraviolet light represents an advantage over other methods. The highest amount of hydrogen obtained for 10%Au@TiO_2-P25 and 3%Au@TiO_2-P25 catalysts was 670 and 583 µmol hg^{-1} respectively, at a wavelength of 400 nm. As it was seen, the surface area of 10%Au@TiO_2-P25 (69 m^2/g) catalyst decreased 14 m^2/g when compared to that obtained by 5%Au@TiO_2-P25.

This reduction on the surface area suggests that the Au NPs are agglomerating on the surface of the catalyst. Yuzawa *et al*. (2012) studied the formation of hydrogen via water splitting under visible light by varying the amount of gold loading (0.1-4.0 wt%) and they established that well dispersed Au NPs decrease the possibility of particle agglomeration, thus enhancing the production of hydrogen. They also concluded that agglomeration of Au NPs can have a detrimental effect since they can act as an active site for the recombination of electron-hole pairs.

For 1%Au@TiO_2-P25 the highest amount of hydrogen was 447 μmol hg^{-1} at a wavelength of 220 nm. Even though the amount of gold loading incorporated was not much when compared to the others, the difference of 293 μmol hg^{-1} obtained between the TiO_2-P25 and 1%Au@TiO_2 P25 catalysts, at a wavelength of 220 nm, is a clear indication of the improvement in the catalytic activity of the composite. The high catalytic activity of the composites can also be appreciated by the amount of hydrogen obtained at wavelengths over 500 nm. At wavelengths of 600 and 700 nm, light does not have enough energy to excite and promote electrons from the valence band to the conduction band of TiO_2, thus, the hydrogen production depends mostly of the incorporated Au NPs.

Figure 14 shows the hydrogen production of the as-synthesized Au@TiO_2 NWs. As can be seen there, the hydrogen production of all titania-gold based catalysts increased greatly when compared to bare TiO_2 NWs. 10%Au@TiO_2 NWs reported the highest production (1,436 μmol hg^{-1}) at 400 nm. This represents a difference of 1,311 μmol hg^{-1} when compared to the highest hydrogen production of the unmodified TiO_2 NWs catalyst (125 μmol hg^{-1}). When the results of the hydrogen production of Au@TiO_2-P25 and Au@TiO_2 NWs are compared, a significantly difference can be appreciated. This result is mainly attributed to the large difference in the surface area of the catalysts (348 m^2/g of difference between 5%Au@TiO_2-P25 and 10%Au@TiO_2 NWs). In the characterization results of Au@TiO_2-P25 it was seen that the surface area decreased when a gold loading of 10 wt% was incorporated to the catalyst; this was not the case with the Au@TiO_2 NWs. That continuous increment in the surface area of the Au@TiO_2 NWs catalysts open the question if higher amounts of hydrogen could be obtained at gold amounts over 10 wt%.

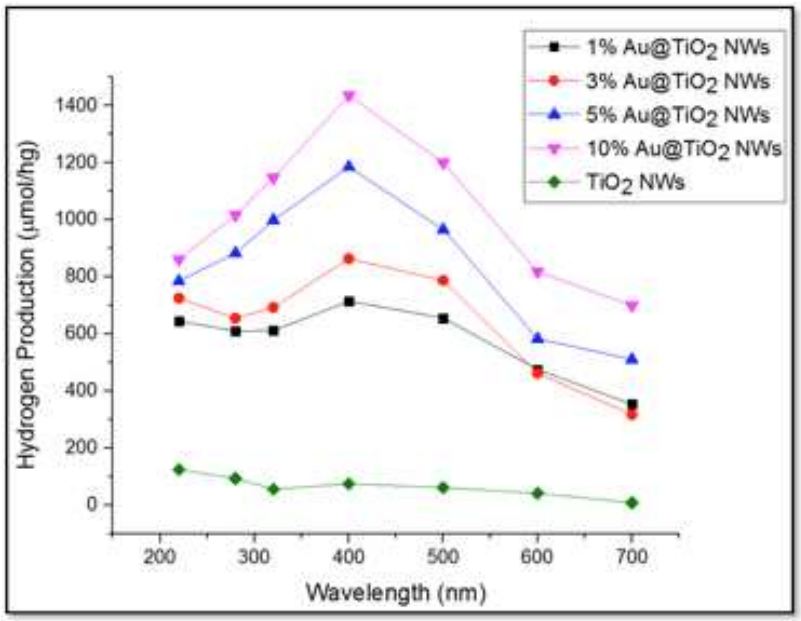

Fig. 14. Hydrogen production for the different Au@TiO_2 NWs catalysts

Table 2. Recent works for photocatalytic hydrogen production using titania gold-based catalysts

Author	H_2 (μmol)	Source (nm)	Irradiation time (h)	Au wt%
[a] Murdoch *et al*. (2011)	660	350	1	4
[b]Gomes-Silva *et al*. (2011)	1211	λ> 400	3	1.5
[c]Jose *et al*. (2013)	1600	254 < λ < 500	5	2
[d] Oros-Ruiz *et al*. (2013)	1866	254	10	0.5
[e]This work	1436 800	400	2	10 5

As it was seen with Au@TiO_2-P25 catalysts, the fact that the highest amount of hydrogen was obtained at 400 nm and not at 220 nm (as it was seen for TiO_2 NWs catalyst) is an indication of the ability of the composites to use visible light. This ability has been ascribed to the presence of Au NPs.

Also at 400 nm, 1%Au@TiO_2 NWs (715 μmol hg^{-1}), 3%Au@TiO_2 NWs (864 μmol hg^{-1}) and 5%Au@TiO_2 NWs (1,186 μmol hg^{-1}) obtained the highest hydrogen productions. At low energy wavelengths (600 and 700 nm), all the catalysts reported amounts of hydrogen above 300 μmol hg^{-1}, demonstrating once again their high catalytic activity. Impressive amounts of 818 and 700 μmol hg^{-1} were obtained with 10%Au@TiO_2 NWs at 600 and 700 nm, respectively.

Table 2 shows some of the most recent results for gold-titania systems, including some of the reaction conditions and the characteristics of the catalysts used in these studies. As can be seen there, the hydrogen production varies depending on different factors, including the reaction conditions, gold loading, nature of the support and irradiation, among others. A comparison of the results reported in the literature is very difficult because of the clear differences in the reaction processes. However, in the catalysts studied in this study, it is important to highlight the large amount of hydrogen produced after only two hours of reaction, compared to previous works.

Conclusion

Gold nanoparticles were incorporated on the synthesized TiO_2 NWs catalysts and the commercial form (TiO_2-P25). These catalysts were fully characterized using SEM, BET, TEM, XRD, Raman and UV-Vis.

In the case of the Au@TiO_2-P25 composites, the highest hydrogen production was 800 μmol hg^{-1} at a wavelength of 400 nm and was obtained with a gold loading of 5 wt%. The enhancement in the hydrogen production was 5.2 times higher than that reported for the TiO_2-P25 catalyst (154 μmol hg^{-1}). The Au NPs deposited on the catalysts allowed the use of visible light and enhanced the hydrogen production in both the visible and ultraviolet regions of the electromagnetic spectrum. At a gold loading of 10 wt%, the catalyst showed a reduction in the surface area as well as in hydrogen production when compared to the 5 wt%. This suggests that the best gold loading for the TiO_2-P25 catalyst ranges from 5 wt% and less than 10 wt%.

The Au@TiO_2 NWs catalysts obtained the highest hydrogen production (1,436 μmol hg^{-1}) at a wavelength of 400 nm and was obtained with a gold loading of 10 wt%. The enhancement in the hydrogen production was 11.5 times higher than that reported by the TiO_2 NWs catalyst (125 μmol hg^{-1}). The Au NPs deposited on the catalysts also allowed the use of visible light and enhanced the hydrogen production in both the visible and ultraviolet regions of the electromagnetic spectrum.

The results obtained in the present investigation indicate that the catalysts based on Au-TiO_2 can represent an efficient alternative for the hydrogen production by water splitting. However, for these processes to be effective, it is still necessary to improve production rates and also to ensure the recyclability of the catalysts.

Acknowledgment

Financial support provided by the US DoE, through the Massie Chair project at University of Turabo, US Department of Defense, under contract W911NF-14-1-0046 and from the Ministerio de Economía y Competitividad (MINECO) of Spain, through the grant ENE2014-57977-C2-1-R, are gratefully acknowledged.

Author's Contributions

All authors contributed equally to this work.

Ethics

Nothing to declare.

References

Baatz, C., N. Decker and U. Prube, 2008. New innovative gold catalysts prepared by an improved incipient wetness method. J. Catal., 258: 165-169. DOI: 10.1016/j.jcat.2008.06.008

Balat, M., 2008. Potential importance of hydrogen as a future solution to environmental and transportation problems. Int. J. Hydrogen Energy, 33: 4013-4029. DOI: 10.1016/j.ijhydene.2008.05.047

Chen, J.J., J.C.S. Wu, P.C. Wu and D.P. Tsai, 2011. Plasmonic photocatalyst for H_2 evolution in photocatalytic water splitting. J. Phys. Chem. C, 115: 210-216. DOI: 10.1021/jp1074048

Cotto, M., T. Campo, E. Elizalde, A. Gómez and C. Morant *et al*., 2013. Photocatalytic degradation of rhodamine-B under UV-visible light irradiation using different nanostructured catalysts. Am. Chem. Sci. J., 3: 178-202. DOI: 10.9734/ACSJ/2013/2712

Dunn, S., 2012. Hydrogen futures: Toward a sustainable energy system. Int. J. Hydrogen Energy, 27: 235-264. DOI: 10.1016/S0360-3199(01)00131-8

Fang, J., S.W. Cao, Z. Wang, M.M. Shahjamali and S.C. Loo *et al*., 2012. Mesoporous plasmonic Au-TiO_2 nanocomposites for efficient visible-light-driven photocatalytic water reduction. Int. J. Hydrogen Energy, 37: 17853-17861. DOI: 10.1016/j.ijhydene.2012.09.023

Fujishima, A. and K. Honda, 1972. Electrochemical photolysis of water at a semiconductor electrode. Nature, 238: 37-38.

Gomes-Silva, C., R. Juárez, T. Marino, R. Molinari and H. García, 2011. Influence of excitation wavelength (UV or visible light) on the photocatalytic activity of titania containing gold nanoparticles for the generation of hydrogen or oxygen from water. J. Am. Chem. Society, 133: 595-602. DOI: 10.1021/ja1086358

Hanoar, D.A.H. and C.C. Sorrell, 2011. Review of the anatase to rutile phase transformation. J. Mater. Sci., 46: 855-874. DOI: 10.1007/s10853-010-5113-0

Haro, M., R. Abargues, I. Herraiz-Cardona, J. Martínez-Pastor and S. Giménez, 2014. Plasmonic versus catalytic effect of gold nanoparticles on mesoporous TiO_2 electrodes for water splitting. Electrochim. Acta, 144: 64-70. DOI: 10.1016/j.electacta.2014.07.146

Haruta, M., T. Kobayashi, H. Sano and L. Yamada, 1987. Novel gold catalysts for the oxidation of carbon monoxide at a temperature far below 0°C. Chem. Lett., 16: 405-408. DOI: 10.1246/cl.1987.405

Jose, D., C.M. Sorensen, S. Rayalu, K.M. Shrestha and K.J. Klabunde, 2013. Au-TiO_2 nanocomposites and efficient photocatalytic hydrogen production under UV-visible and visible light illuminations: A comparison of different crystalline forms of TiO_2. Int. J. Photoenergy, 2013: 685614-685614.

Kowalska, E., S. Rau and B. Ohtani, 2012. Plasmonic titania photocatalysts active under UV and visible-light irradiation: influence of gold amount, size and shape. J. Nanotechnol., 2012: 361853-361863. DOI: 10.1155/2012/361853

Kudo, A. and Y. Miseki, 2008. Heterogeneous photocatalyst materials for water splitting. Chem. Society Rev., 38: 253-278. DOI: 10.1039/B800489G

Kuo, Y., C.D. Frye, M. Ikenberry and K.J. Klabunde, 2013. Titanium-indium oxy(nitride) with and without RuO_2 loading as photocatalysts for hydrogen production under visible light from water. Catalisis Today, 199: 15-21. DOI: 10.1016/j.cattod.2012.03.012

Lakshminarasimhan, N., E. Bae and W. Choi, 2007. Enhanced photocatalytic production of H_2 on Mesoporous TiO_2 prepared by template-free method: Role of interparticle charge transfer. J. Phys. Chem. C, 111: 15244-15250. DOI: 10.1021/jp0752724

Li, R., Y. Weng, X. Zhou, X. Wang and M. Yang *et al*., 2015. Achieving overall water splitting using titanium dioxide-based photocatalysts of different phases. Energy Environ. Sci., 8: 2377-2382. DOI: 10.1039/C5EE01398D

Liao, C.H., C.W. Huang and J.C.S. Wu, 2012. Hydrogen production from semiconductor-based photocatalysis via water splitting. Catalysts, 2: 490-516. DOI: 10.3390/catal2040490

Lin, C., K. Tao, D. Hua, Z. Ma and S. Zhou, 2013. Size effect of gold nanoparticles in catalytic reduction of *p*-Nitrophenol with $NaBH_4$. Molecules, 18: 12609-12620. DOI: 10.3390/molecules181012609

Lu, Y., H. Yu, S. Chen, X. Quan and H. Zhao, 2012. Integrating plasmonic nanoparticles with TiO_2 photonic crystal for enhancement of visible-light-driven photocatalysis. Environ. Sci. Technol., 46: 1724-1730. DOI: 10.1021/es202669y

Luo, J., D. Li, Y. Yang, H. Liu and J. Chen *et al*., 2016. Preparation of Au/reduced graphene oxide/hydrogenated TiO_2 nanotube arrays ternary composites for visible-light-driven photoelectrochemical water splitting. J. Alloys Compounds, 661: 380-388. DOI: 10.1016/j.jallcom.2015.11.211

Luttrell, T., S. Halpegamage, J. Tao, A. Kramer and E. Sutter *et al*., 2014. Why is anatase a better photocatalyst than rutile? Model studies on epitaxial TiO_2 films. Scientific Rep., 4: 1-8.

Manveen, K. and N.K. Verma, 2014. $CaCO_3/TiO_2$ nanoparticles based dye sensitized solar cell. J. Mater. Sci. Technol., 30: 328-334. DOI: 10.1016/j.jmst.2013.10.016

Mazloomi, K. and C. Gomes, 2012. Hydrogen as an energy carrier: Prospects and challenges. Renewable Sustainable Energy Rev., 16: 3024-3033. DOI: 10.1016/j.rser.2012.02.028

Murdoch, M., G.I.N. Waterhouse, M.A. Nadeem, M.A. Metson and M.A. Keane *et al*., 2011. The effect of gold loading and particle size on photocatalytic hydrogen production from ethanol over Au/TiO_2 nanoparticles. Nature Chem., 3: 489-492. DOI: 10.1038/nchem.1048

Naldoni, A., M. D'Arienzo, M. Altomare, M. Marelli and R. Scotti, 2013. Pt and Au/TiO_2 photocatalysts for methanol reforming: Role of metal nanoparticles in tuning charge trapping properties and photoefficiency. Applied Catal. B: Environ., 130: 239-248. DOI: 10.1016/j.apcatb.2012.11.006

Naseri, N., P. Sangpour and A.Z. Moshfegh, 2011. Visible light active Au:TiO_2 nanocomposite photoanodes for water splitting: Sol-gel Vs. sputtering. Electrochim. Acta, 56: 1150-1158. DOI: 10.1016/j.electacta.2010.10.080

Nijishima, Y., K. Ueno, Y. Yokota, K. Murakoshi and H. Misawa, 2010. Plasmon-assisted photocurrent generation from visible to near-infrared wavelength using a Au-nanorods/TiO_2 electrode. J. Phys. Chem. Lett., 1: 2031-2036. DOI: 10.1021/jz1006675

Oros-Ruiz, S., R. Zanella, R. López, A. Hernández and R. Gómez, 2013. Photocatalytic hydrogen production by water/methanol decomposition using Au/TiO_2 prepared by deposition-precipitation with urea. J. Hazardous Mater., 263: 2-10. DOI: 10.1016/j.jhazmat.2013.03.057

Ortega, J., C.R. López, E. Pulido, O. González and J.M. Doña *et al*., 2014. Production of hydrogen by water photo-splitting over commercial and synthesised Au/TiO_2 catalysts. Applied Catal. B: Environ., 147: 439-452. DOI: 10.1016/j.apcatb.2013.09.029

Padikkaparambil, S., B. Narayanan, Z. Yaakob, S. Viswanathan and S. Masrinda, 2013. Au/TiO_2 reusable photocatalyst for dye degradation. Int. J. Photoenergy, 2013: 752605-752605.

Primo, A., A. Corma and H. García, 2011. Titania supported gold nanoparticles as photocatalyst. Phys. Chem. Chem. Phys., 13: 886-910. DOI: 10.1039/C0CP00917B

Shen, P., S. Zhao, D. Su, Y. Li and A. Orlov, 2012. Outstanding activity of sub-nm Au clusters for photocatalytic hydrogen production. Applied Catal. B: Environ., 126: 153-160. DOI: 10.1016/j.apcatb.2012.07.021

Singh, G.P., K.M. Shrestha, A. Nepal, K.J. Klabunde and C.M. Sorensen, 2014. Graphene supported plasmonic photocatalyst for hydrogen evolution in photocatalytic water splitting. Nanotechnol. 25: 265701-265712. DOI: 10.1088/0957-4484/25/26/265701

Stroyuk, A.L., A.I. Kryukov, S.Y. Kuchmii and V.D. Pokhodenko, 2009. Semiconductor photocatalytic systems for the production of hydrogen by the action of visible light. Theoretical Exp. Chem., 45: 199-222. DOI: 10.1007/s11237-009-9095-4

Tamm, A., I.O. Acik, T. Arroval, A. Kasikov and H. Seemen *et al*., 2016. Plasmon resonance effect caused by gold nanoparticles formed on titanium oxide films. Thin Solid Films, 616: 449-455. DOI: 10.1016/j.tsf.2016.08.059

Tanaka, A., S. Sakaguchi, K. Hashimoto and H. Kominam, 2012. Preparation of Au/TiO_2 exhibiting strong surface plasmon resonance effective for photoinduced hydrogen formation from organic and inorganic compounds under irradiation of visible light. Catal. Sci. Technol., 2: 907-909. DOI: 10.1039/C2CY20108A

Wang, H., J.L. Faria, S. Dong and Y. Chang, 2012. Mesoporous Au/TiO_2 composites preparation, characterization and photocatalytic properties. Mater. Sci. Eng.: B, 177: 913-919. DOI: 10.1016/j.mseb.2012.04.015

Yuzawa, H., T. Yoshida and H. Yoshida, 2012. Gold nanoparticles on titanium oxide effective for photocatalytic hydrogen formation under visible light. Applied Catal. B: Environ., 115: 294-302. DOI: 10.1016/j.apcatb.2011.12.029